

Supplemental Information

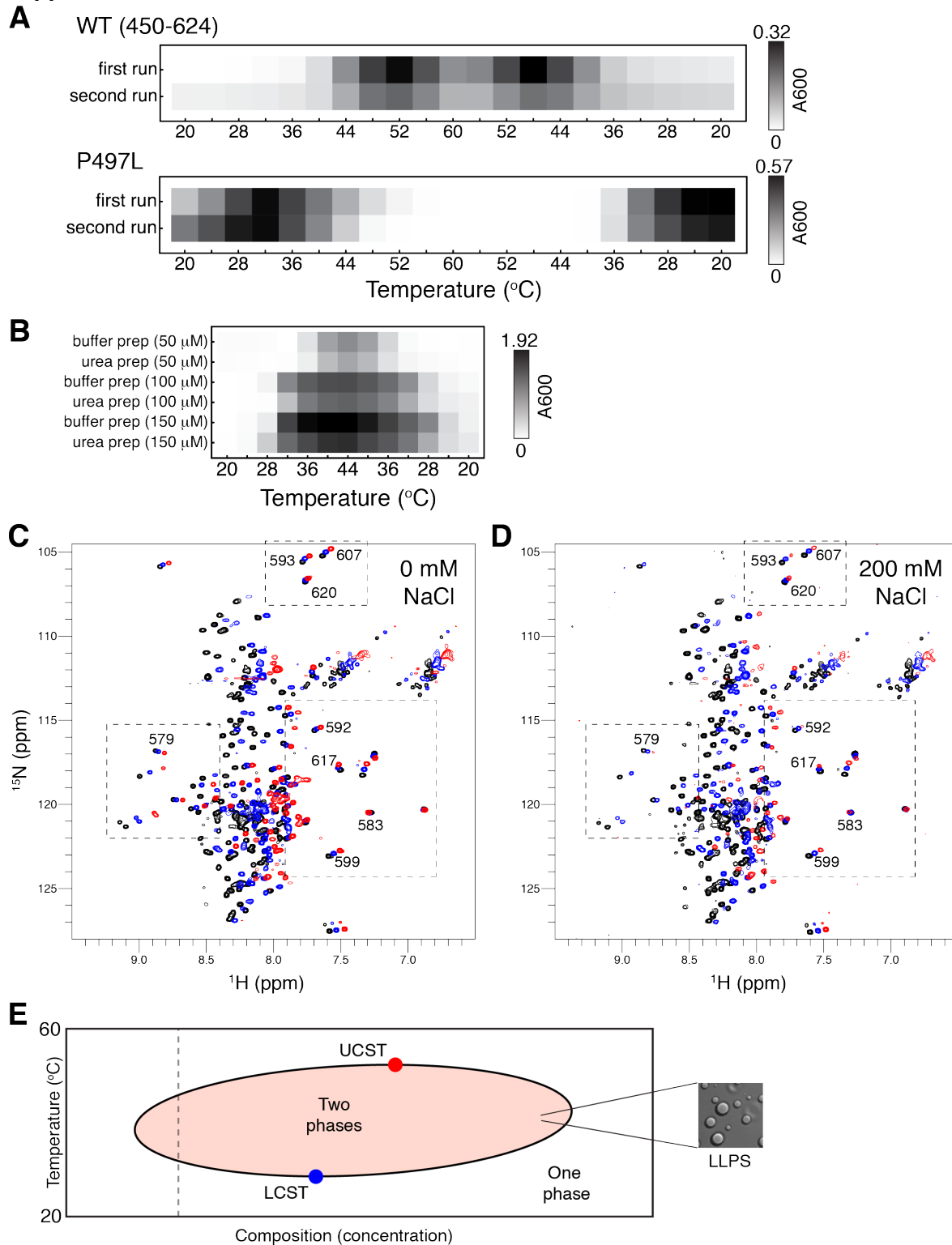


Figure S1. UBQLN2 LLPS is reversible. Related to Figure 1. (A) Spectrophotometric turbidity assay of WT and P497L where the identical 25 μ M protein sample was subjected to two rounds of temperature ramping between 20°C and 60°C. See STAR Methods for details. (B) Spectrophotometric turbidity assay of WT protein (at indicated protein concentrations) with a

temperature ramp between 20°C and 44°C. Here, samples were incubated at indicated temperatures for 2 minutes, before switching to next temperature. All protein samples were in pH 6.8 buffer consisting of 20 mM NaPhosphate and 200 mM NaCl. (C,D) ^1H - ^{15}N CP-HISQC NMR spectra of 50 μM UBQLN2 collected at 25°C (black), 40 °C (blue), and 55°C (red) in pH 6.8 buffer containing 20 mM NaPhosphate, with no added NaCl (C) and 200 mM NaCl (D). Experiment acquisition parameters and contour settings are identical for each set of spectra in (C) and (D). Representative UBA peaks are denoted by dashed boxes and labeled with corresponding residue number. (E) Schematic of LCST-UCST closed-loop phase diagram illustrating how UBQLN2 undergoes two phase transitions between 20°C and 60°C at a particular protein concentration (dotted line). LCST and UCST are lower critical solution temperature and upper critical solution temperature, respectively.

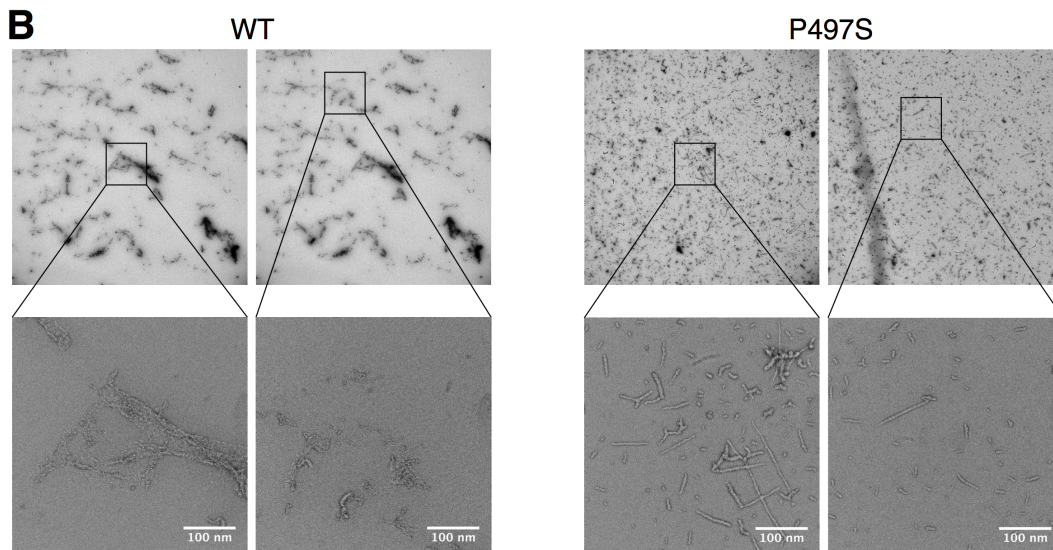
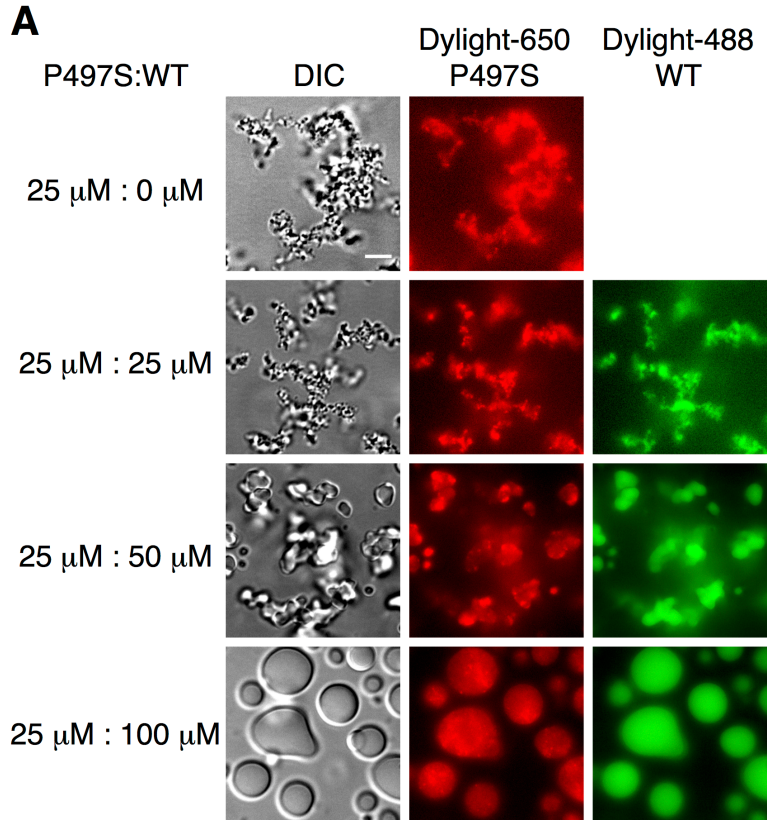


Figure S2. WT colocalizes with P497S aggregates. Related to Figure 1. (A) WT and P497S proteins were fluorescently-tagged on their N-termini with DyLight-488 and Dylight-650, respectively (see STAR Methods). Different ratios of protein were mixed and subsequently imaged. Scale bar = 5 μ m. (B) Transmission electron microscopy of WT and P497S 450-624 constructs after phase separation is induced at 60 μ M protein, 200 mM NaCl, 20 mM Tris pH 7.4, then diluted 1:20 into 20 mM Tris pH 7.4 buffer immediately before staining. Note that WT was largely devoid of any discernible aggregates or fibrils, except for the panel shown here. Filamentous structures were present in nearly all P497S panels.

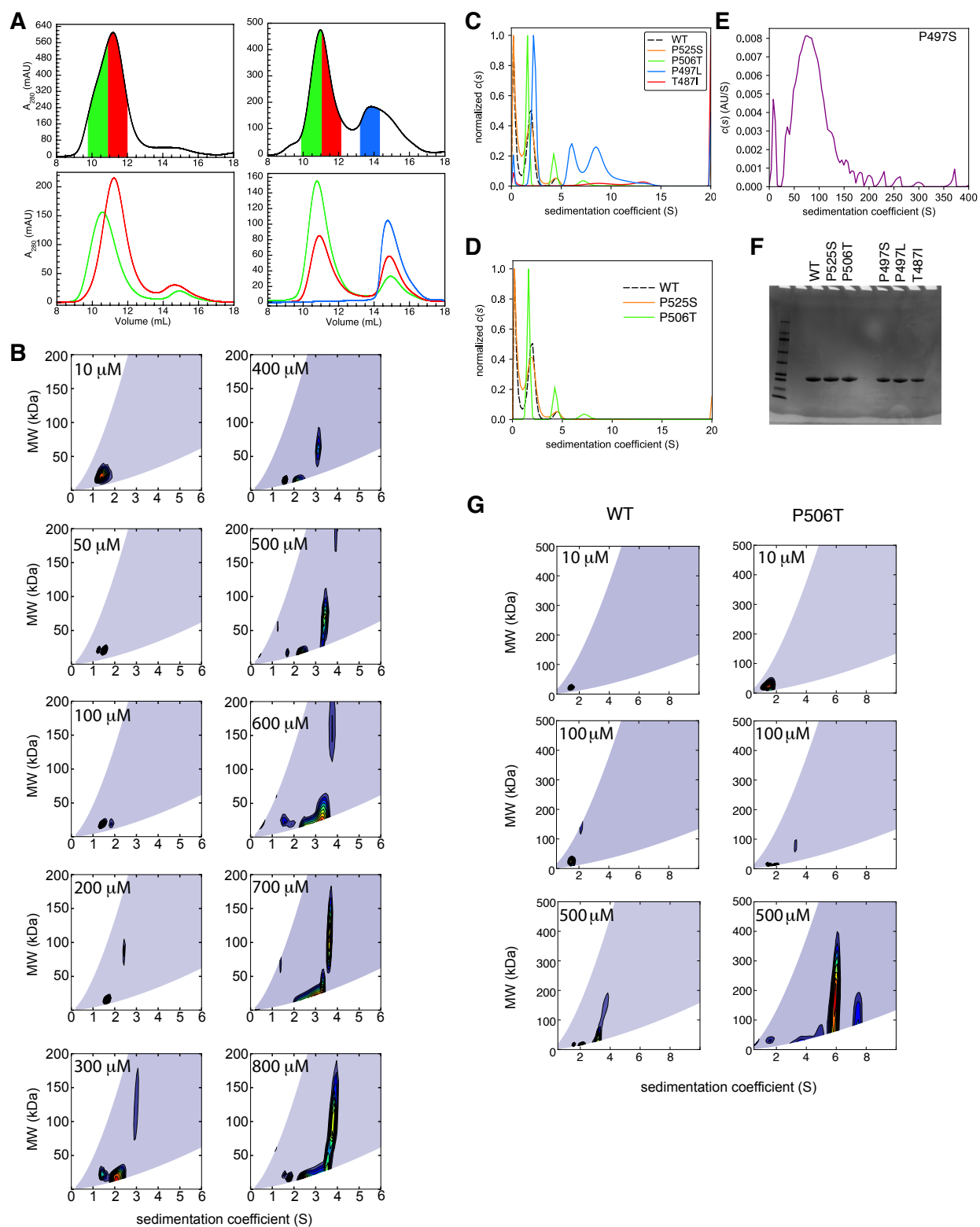


Figure S3. SEC and AUC studies of UBQLN2 mutants. Related to Figure 3. (A) SEC of UBQLN2 Pxx mutants T487I (left) and P497L (right) at 500 μ M protein concentration (top panel) and the fractions collected from the aforementioned SEC runs (bottom panels). (B) Contour

plots of a two-dimensional distribution of molar mass (MW) and sedimentation coefficients (S) for WT UBQLN2 between 10 and 800 μM (C) Overlay of normalized coefficient distribution $c(s)$ plots for WT and Pxx mutants using 100 μM protein at 25°C in buffer containing 20 mM NaPhosphate (pH 6.8) with no added NaCl. (D) Overlay of Pxx mutants that behave similarly to WT. (E) $c(s)$ plot for 100 μM P497S over sedimentation range up to 400S. (F) SDS-PAGE gel of AUC samples post-run. (G) Contour plots of a two-dimensional distribution of molar mass (MW) and sedimentation coefficients (S) comparing WT UBQLN2 and P506T at 10, 100 and 500 μM concentrations.

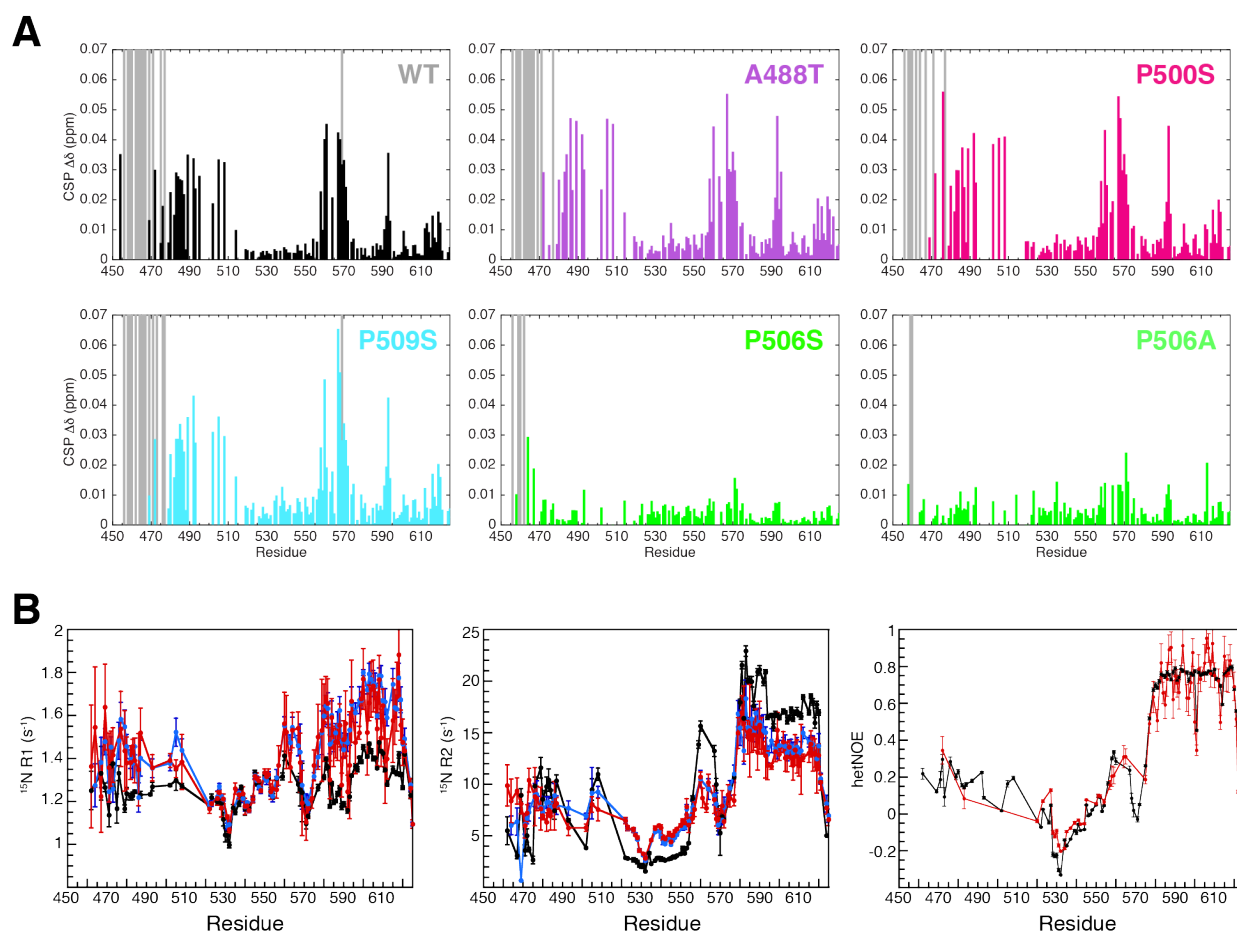


Figure S4. NMR studies of UBQLN2 mutants. Related to Figure 5. (A) Concentration-dependent CSPs for Pxx mutants not displayed in Figure 5A. Gray bars denote those resonances that are broadened beyond detection at high protein concentration (350 μM). Plots are organized and color-coded to match the arrangement in Figures 1 and 3. (B) ^{15}N R1 and R2 relaxation rates and $\{^1\text{H}\}$ - ^{15}N hetNOE values for WT (black), P497L (blue), and T487I (red) proteins at 200 μM protein concentration. Errors in ^{15}N R1 and R2 relaxation rates were determined using 500 Monte Carlo trials in RELAXFIT (see STAR Methods).

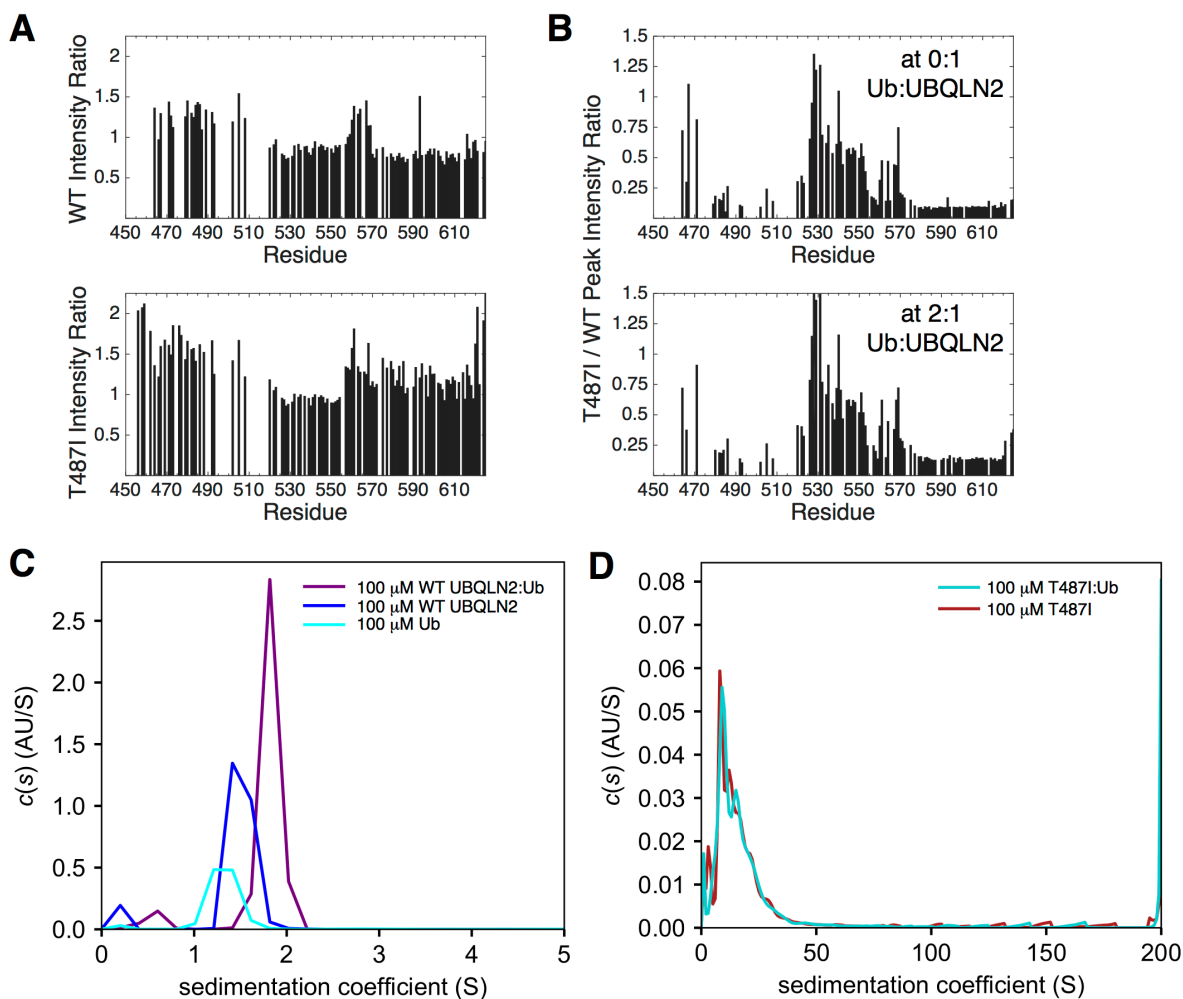


Figure S5. UBQLN2 oligomerization is not disrupted by Ub binding. Related to Figure 6. (A) Ratio of amide peak intensities between titration endpoints (2:1 Ub:UBQLN2 and 0:1 Ub:UBQLN2) using 200 μ M UBQLN2 WT protein (top) or T487I mutant (bottom). (B) Ratio of amide peak intensities between T487I and WT UBQLN2 at two different titration endpoints (top: beginning, bottom: end). (C,D) Diffusion-free sedimentation coefficient distribution $c(s)$ plots for (C) WT UBQLN2 and (D) T487I in the absence and presence of Ub, at 100 μ M protein concentration under non-phase separating conditions (no added NaCl) from SV-AUC experiments.

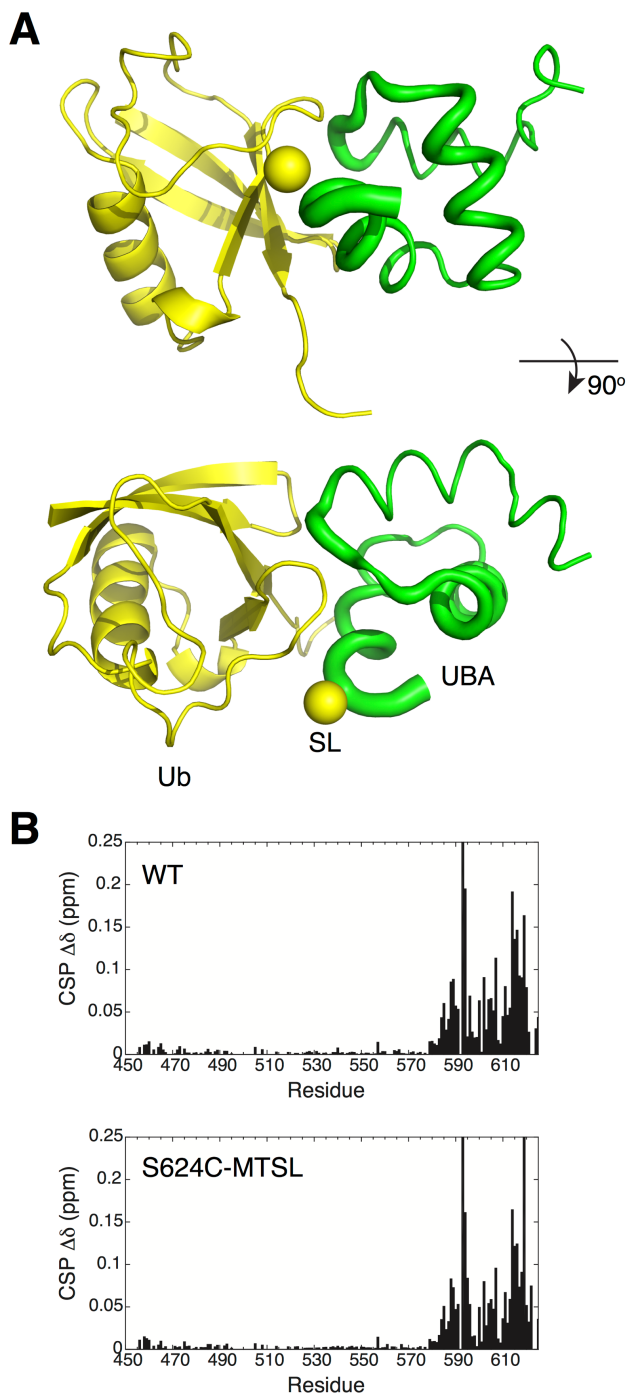


Figure S6. S624C spin label does not perturb ubiquitin (Ub) binding. Related to Figure 7. (A) Model of UBQLN2 UBA:Ub binding using PDB: 2JY6 (see STAR Methods). Position of spin label was determined in the free UBA state. The UBA and ubiquitin proteins are colored green and yellow, respectively, with UBA ribbon thickness denoting high PRE effects (low I/I_0 values, see Figure 7A). Yellow sphere (SL) represents back-calculated position of the S624C spin label on the UBA domain. (B) Chemical shift perturbations (CSPs) upon binding Ub (50 μ M) in a 1:1 molar ratio with WT (top) or S624C with attached MTSL spin label in the reduced state.

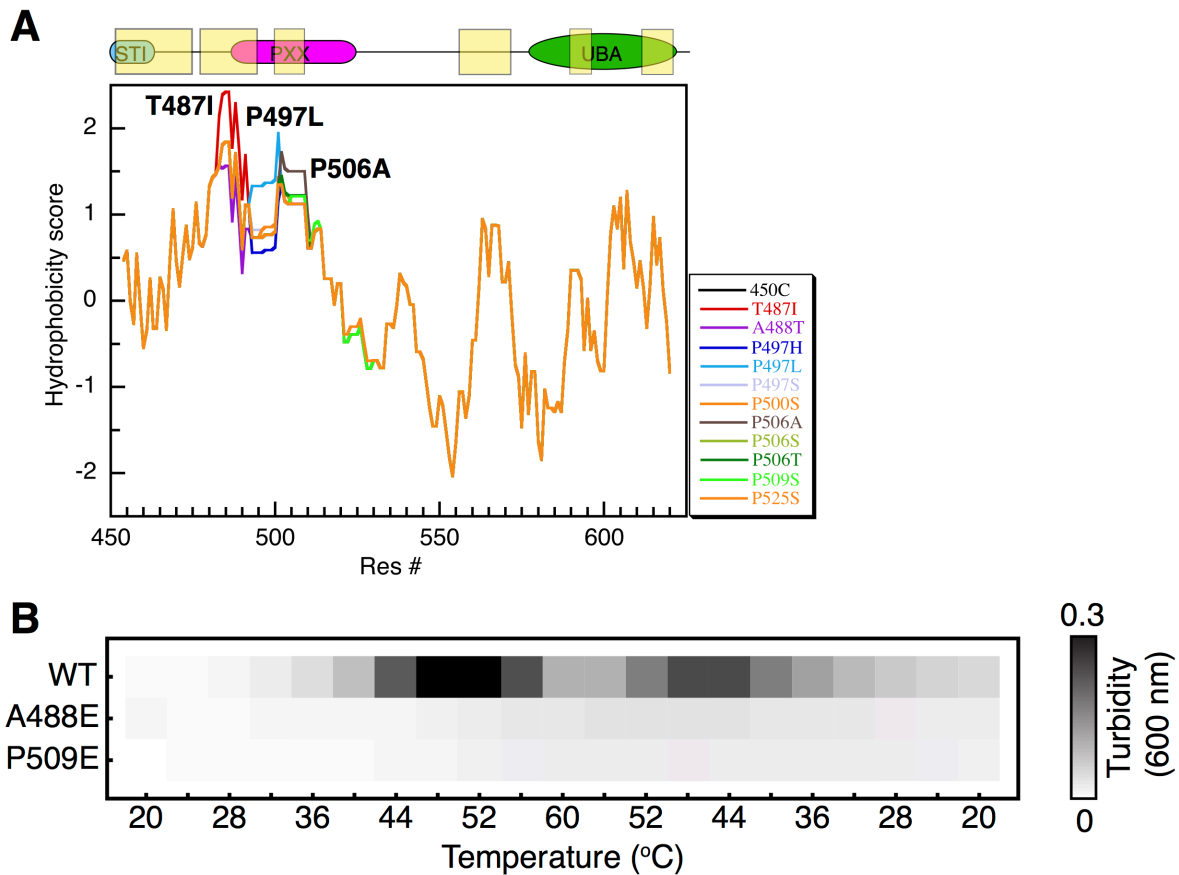


Figure S7. (A) Residue-by-residue hydropathy plots for UBQLN2 450-624 and Pxx mutants. Related to Figure 7. Domain map is shown above the plot with translucent yellow boxes denoting concentration-dependent CSPs for WT UBQLN2 that may mediate UBQLN2 LLPS (see Figure 5A and (Dao et al., 2018)). Pxx mutants with increased hydrophobicity are noted in black. (B) Results from spectrophotometric turbidity assay as a function of temperature comparing LLPS of UBQLN2 A488E and P509E mutants to WT using 25 μ M protein in 20 mM NaPhosphate and 200 mM NaCl (pH 6.8).